Photoelectron ionization time of aligned molecules clocked by attosecond angular streaking

Jiaqing Yan,[1] Wenhai Xie,[1] Min Li,[1,*] Kun Liu,[1] Siqiang Luo,[1] Chuanpeng Cao,[1] Keyu Guo,[1] Wei Cao,[1] Pengfei Lan,[1] Qingbin Zhang,[1] Yueming Zhou,[1] and Peixiang Lu[1,2,3,†]

[1]*Wuhan National Laboratory for Optoelectronics and School of Physics, Huazhong University of Science and Technology, Wuhan 430074, China*

[2]*Hubei Key Laboratory of Optical Information and Pattern Recognition, Wuhan Institute of Technology, Wuhan 430205, China*

[3]*CAS Center for Excellence in Ultra-intense Laser Science, Shanghai 201800, China*

(Received 6 July 2020; accepted 8 July 2020; published 31 July 2020)

Attoclock is a powerful technique to resolve laser-driven electron dynamics on an attosecond time scale. Previously, it was mainly limited to atomic targets. Here we apply the attoclock technique to aligned molecules to study the subcycle ionization dynamics. By controlling the alignment of the molecule relative to the major axis of a strong elliptically polarized laser field, we demonstrate that the electron ionization time in aligned molecules can be precisely resolved by the attoclock technique. We find that the ionization time corresponding to the peak of the photoelectron momentum distribution shifts several tens of attoseconds relative to the laser field peak depending on the molecular orientation and molecular orbital structure. A significant difference between the measurement and molecular Ammosov-Delone-Krainov model is found. We further show that the photoelectron ionization time of molecules is sensitive to angular-dependent ionization rate, opening up opportunities for probing attosecond electron dynamics in complex polyatomic molecules.

DOI: 10.1103/PhysRevA.102.013117

I. INTRODUCTION

The advent of attosecond metrology has opened possibilities to detect and resolve electron dynamics in atoms and molecules with an extremely high temporal resolution, which is at the forefront of attosecond science [1]. The attoclock, or attosecond angular streaking, is a recently developed technique that accesses such short time scales based on strong-field tunneling ionization [2]. In the attoclock technique, a strong close to circularly polarized femtosecond laser pulse is utilized to map the subcycle emission time of an electron to its detection angle. Since strong-field tunneling is a highly nonlinear process, the ionization is confined to subfemtosecond intervals near the peak of the laser field with releasing an electron wave packet. The rotating electric field of the femtosecond laser subsequently exerts a force on the emitted electron that varies on a subfemtosecond scale. Analogous to a conventional streaking camera, attosecond timing precision and resolution can be achieved without relying on the existence of attosecond pulses; e.g., a time resolution of $\sim$7 as can be achieved for a resolution of 1° in the emission angle using an 800-nm laser field. In typical attoclock experiments, the electron emission angle in the photoelectron momentum distribution (PMD) is measured at which the ionization probability is maximum. For an atom, this emission angle corresponds to the laser electric-field peak since the tunneling ionization is an exponentially suppressed process [3]. So far, the emission angle has been used to precisely measure the tunneling delay time and initial coordinates of quantum tunneling for atoms [2–9]. In the attoclock technique, disentangling the effect of the ionic Coulomb potential on the electron emission angle is a difficult task, which has a significant impact on the interpretation of attoclock experiments [9].

Compared to atoms, molecules have an anisotropic electrostatic potential arising from the molecular geometry. This anisotropic potential and the external field form different tunneling barriers for the bound electron when the molecular axes are oriented in different directions, which will modify the ionization process [10–12] and will further complicate the interpretation of attoclock experiments. Several rudimentary attoclock experiments on molecules were reported for dissociative ionization of H_2 [13,14], in which the electron was detected in coincidence with the fragment ion. Recently, by detecting all ionic fragments, an upper bound of 10 as on the tunneling delay time has been given for H_2 using the attoclock technique [15]. Additionally, the attoclock method has also been used to reveal electron correlation dynamics in double ionization of benzene [16]. However, in those studies, the molecules were not aligned and the alignment dependence of the subcycle ionization dynamics in molecules was unexplored.

In this paper, we employ the attoclock method to resolve the subcycle ionization time of photoelectrons in strong-field tunneling ionization of laser-aligned N_2 and CO_2 molecules. By measuring the alignment-dependent photoelectron angular distributions (PADs) in the attoclock configuration, we find that the emission angle for the most probable electron trajectory oscillates as a function of the molecular alignment angle. Because the Coulomb effect on the photoelectron is nearly the same for different molecular orientations, the measured photoelectron emission angles allow us to directly resolve the ionization time corresponding to the peak of the PMD

*mli@hust.edu.cn
†lupeixiang@hust.edu.cn

for different orientations without counting on the theoretical modeling of the Coulomb effect. The extracted photoelectron ionization time shows a significant disagreement with the prediction of the molecular Ammosov-Delone-Krainov (MO-ADK) model [17], revealing a sensitive dependence on the angular ionization rate of the molecule. We further analyze the alignment dependence of the angular width of the PAD, which is strongly affected by the molecular orbital structure. A clear signature of two-center electron interference is observed, confirming the prediction by Serov *et al.* [18].

II. METHODS

A. Experimental setup

Experimentally, the laser pulse was generated by an amplified Ti:sapphire femtosecond laser system centered at 800 nm with a repetition rate of 5 kHz and a pulse duration of about 40 fs. It was split in a Michelson interferometer into an alignment pulse and a probe pulse with an adjustable delay. The duration of the alignment pulse was stretched to about 100 fs through an SF11 glass with a thickness of ∼8 mm. Then the alignment and probe beams were recombined and focused by a $f = 75$ mm parabolic mirror into a continuous N_2 or CO_2 supersonically cooled gas jet. The three-dimensional momenta of the resulting photoelectrons were detected using cold target recoil ion momentum spectroscopy (COLTRIMS) [19,20].

B. Molecule alignment

In order to generate a macroscopic field-free alignment for the molecules around the polarization axis of the alignment pulse, we set the time delay between the probe pulse and the alignment pulse to be ∼8.33 and ∼21.1 ps for N_2 and CO_2 [21,22], respectively. The probe pulse was elliptically polarized while the alignment pulse was linearly polarized. The alignment laser beam had a motorized half-wave plate continuously changing the alignment direction relative to the major axis of the elliptically polarized probe pulse. To calibrate the ellipticity and the intensity of the probe pulse, we further measured the PMD of the Ar atom with the same probe pulse and compared the measured PMD of Ar with classical-trajectory Monte Carlo simulations, in which the nonadiabatic effect has been considered [23–25]. The degrees of the alignment for the molecules were obtained by solving the time-dependent Schrödinger equation based on the rigid rotor model [26,27] (see Appendix A for more details).

III. RESULTS AND DISCUSSIONS

Figure 1 shows the measured PMDs for N_2 molecules with alignment angles of 45° and 135° ionized by the same elliptically polarized laser pulse. k_x and k_y are the electron momenta along the major and minor axes of the laser ellipse, respectively. The alignment angle θ is defined between molecular axis direction relative to the major axis of the laser ellipse. The weak signals with $|k_y| < 0.4$ a.u. come from the ionization from the alignment laser pulse, which could be regarded as a marker for the molecular axis alignment direction. One can clearly see that the PMDs are very different for

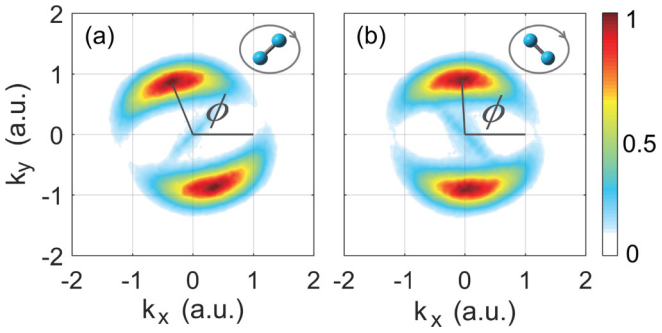

FIG. 1. The measured PMDs in the polarization plane of an elliptically polarized laser pulse for N_2 molecules with alignment angles of (a) 45° and (b) 135°. The angle ϕ is defined between the electron emission direction relative to the major axis of the laser ellipse. The laser intensity and ellipticity are $\sim 1.8 \times 10^{14}$ W/cm^2 and ∼0.82, respectively.

different alignment angles. The emission angle ϕ for the most probable electron trajectory is almost 112° for the alignment angle of 45°, while it shifts to ∼95° for the alignment angle of 135°. This implies that the emission angle of the photoelectron depends on the molecular orientation.

To shed light on the alignment dependence of the photoelectron emission angle, we show in Figs. 2(a) and 2(b) the momentum-integrated PADs as a function of the alignment angle for N_2 and CO_2, respectively. The photoelectron yields in the PADs oscillate obviously with the alignment angle for

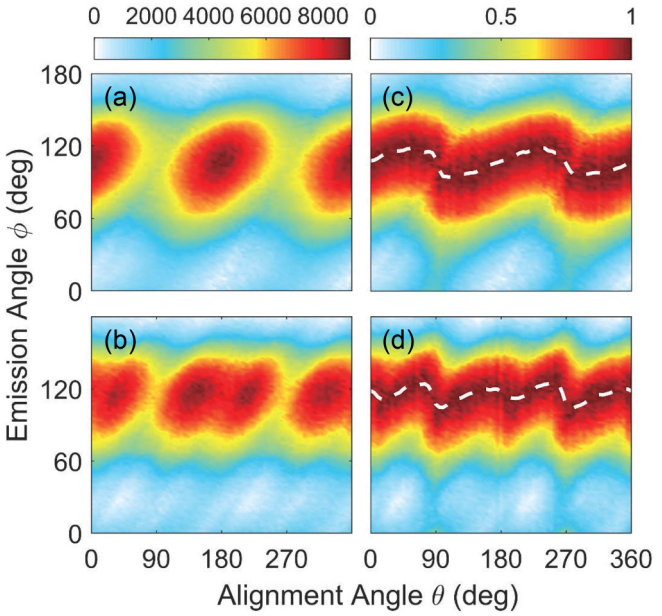

FIG. 2. The measured momentum-integrated PADs with respect to the alignment angle relative to the major axis of the laser ellipse for (a) N_2 and (b) CO_2. (c), (d) The same as in (a) and (b) but normalized to maximum at each alignment angle. The white dashed lines in (c) and (d) are used to guide the emission angle for the most probable electron trajectory at each alignment angle. The laser intensities (ellipticities) and the degrees of alignment are, respectively, (a) 1.8×10^{14} W/cm^2 ($\epsilon = 0.82$), 0.65; (b) 1.6×10^{14} W/cm^2 ($\epsilon = 0.85$), 0.60.

both molecules. Interestingly, the oscillation of the photoelectron yield reveals a single-peak structure within the alignment angle range of (90°, 270°) for N_2 while it splits into a double-peak structure for CO_2 within the same alignment angle range. This reflects the symmetry of the highest occupied molecular orbital (HOMO) for N_2 (σ_g) and CO_2 (π_g) [21]. To clearly see the change of the emission angle for the most probable trajectory, we normalize the PAD at each alignment angle to the maximum, as shown in Figs. 2(c) and 2(d). One can see that the emission angle for the most probable trajectory also oscillates with the molecular alignment angle, as guided by the white dashed lines. Similar to the photoelectron yield, the oscillation of the emission angle with respect to the alignment angle also reveals a single-peak structure within the alignment angle range (90°, 270°) for N_2, while a double-peak structure appears for CO_2.

According to the attoclock principle, the emission angle of an electron in a close to circularly polarized laser field is directly related to its emission time $t_0(\theta)$ by the momentum-to-time mapping [2,8,9] [atomic units (a.u.) are used throughout unless stated otherwise]

$$\phi(\theta) = \frac{\omega t_0(\theta)}{\epsilon} + \phi^{cc} + \frac{\pi}{2}, \tag{1}$$

where ω and ϵ are the frequency and ellipticity of the laser field, respectively. The factor $\pi/2$ comes from the fact that the vector potential trails the rotating electric field by 90° at the laser field peak ($t_0 = 0$), corresponding to the major axis of the laser ellipse. ϕ^{cc} is the angular offset arising from the Coulomb effect on the electron. Because the electron is released at the tunnel exit away from the ionic cores, the Coulomb correction to the emission angle ϕ^{cc} is nearly the same for different molecular alignments; as demonstrated by the electron trajectories in Appendix B, this angle is already lower than the experimental accuracy. Thus the photoemission time $t_0(\theta)$ corresponding to the peak of the PMD can be directly resolved from the measured emission angle $\phi(\theta)$ without relying on the theoretical modeling of the Coulomb effect. In Figs. 3(a) and 3(b), we plot the emission angle for the most probable electron trajectory as a function of the alignment angle for N_2 and CO_2, respectively. Here the measured emission angle is shifted to near zero to rule out the effect of the last two terms of Eq. (1). We see that the emission angle oscillates as a function of the alignment angle with an amplitude of ~12° for both N_2 and CO_2, corresponding to a shift of almost ±80 as for the ionization time corresponding to the peak of the PMD relative to the field peak according to Eq. (1).

The shift of the ionization time corresponding to the peak of the PMD relative to the field peak for molecules can be qualitatively explained using the notion of instantaneous ionization rate [28]. For a molecule, though the instantaneous ionization rate is dominated by the instantaneous electric field of the laser, it is also strongly influenced by the molecular orbital. In a near circularly polarized laser pulse, the instantaneous electric field varies slowly with time. As a result, the effect of the molecular orbital on the instantaneous ionization rate becomes important. Due to the anisotropy of the molecular orbital, the interplay of the instantaneous electric field and the molecular orbital structure leads to a shift of the ionization

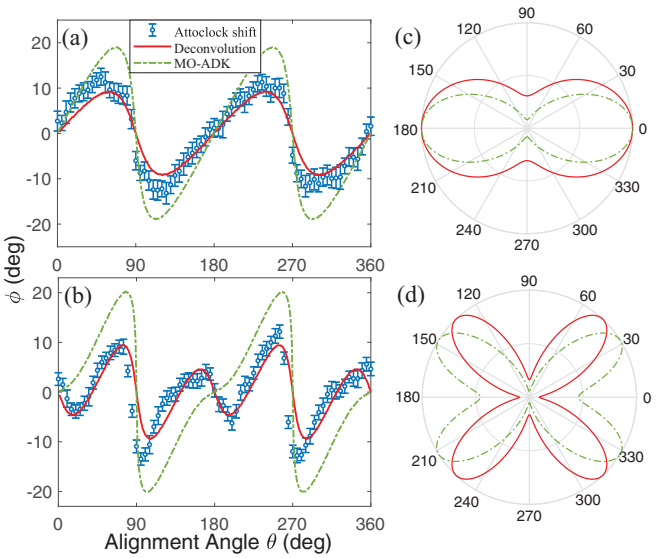

FIG. 3. The photoelectron emission angle for the most probable trajectory with respect to the alignment angle for (a) N_2 and (b) CO_2. The dash-dotted lines are the predictions of the MO-ADK model, and the solid red lines are calculated using the angular-dependent ionization rate after deconvolution with the alignment distribution. The solid red lines in (c) and (d) are the angular-dependent ionization rate after deconvolution with the alignment distribution for (c) N_2 and (d) CO_2. The corresponding MO-ADK results are shown by the dashed dotted lines for comparison.

time corresponding to the peak of the PMD with respect to the field peak.

Next we compare the measured photoelectron ionization time with the prediction of the MO-ADK model [17]. As shown by the dash-dotted lines in Figs. 3(a) and 3(b), one can see that the predictions of the MO-ADK model deviate noticeably from the measurements. The amplitudes of the oscillations predicted by the MO-ADK model are close to 20° for both molecules, which are much larger than the measurements. In particular, the double-peak structure of CO_2 does not appear in the MO-ADK result within the alignment angle range (90°, 270°). Note the effect of the alignment distribution has been included in the simulations.

To understand the difference between the measurement and the MO-ADK result, we investigate the instantaneous ionization rate of a molecule in a close to circularly polarized laser field, which can be approximately given by $S(t_0, \theta) = W(t_0)S(\theta)$. Here $S(\theta)$ is the angular-dependent ionization rate related to the molecular orbital structure, and $W(t_0)$ is related to the instantaneous electric field of the laser pulse, which can be estimated using the atomic ADK ionization rate [29]. The angular dependence of the ionization rate $S(\theta)$ predicted by the MO-ADK model is shown by the dash-dotted lines in Figs. 3(c) and 3(d). Previously, it was shown that the angular-dependent ionization rate predicted by the MO-ADK model has a significant disagreement with the measurement [21,22], which was subsequently explained by the effect of multiple ionizing orbitals [30], multielectron effects [31], exchange interactions [32], the interplay of coordinate- and momentum-space properties of the ionizing orbital [33], or laser-induced

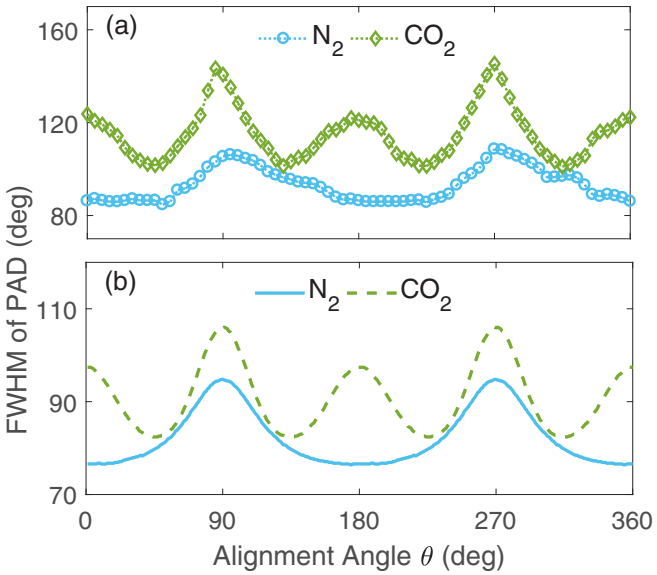

FIG. 4. The FWHM of the PAD with respect to the alignment angle for N_2 and CO_2 from the measurement (a) and the simulation (b).

orbital deformation [34]. Since those explanations remain as yet unconfirmed, we follow the deconvolution method in Ref. [21] to obtain an accurate angular-dependent ionization rate from the measured alignment-dependent electron yields [Figs. 2(a) and 2(b)]. The details of the deconvolution process are presented in Appendix C. As shown by the solid red lines in Fig. 3(c), the angular-dependent ionization rate using the deconvolution method for N_2 is less peaked than the one predicted by the MO-ADK model. The ionization is about three times higher for $\theta = 0^\circ$ than for $\theta = 90^\circ$, consistent with previous studies [21]. The MO-ADK theory predicts 10:1 for $\theta = 0^\circ$ vs $\theta = 90^\circ$ ratio. In the case of CO_2, the angular-dependent ionization rate after the deconvolution [solid red line in Fig. 3(d)] is peaked at about $\theta = 45^\circ$ with little ionization at $\theta = 0^\circ$ and $\theta = 90^\circ$, while the MO-ADK model predicts that the ionization rate peaks at $\theta = 30^\circ$. This result also agrees with previous studies [21,35]. Using the deconvoluted angular-dependent ionization rate, we achieve an agreement with the measured emission angles for both N_2 and CO_2, as shown by the solid red lines in Figs. 3(a) and 3(b). Comparing the result from the deconvolution method with the MO-ADK result in Fig. 3, we can find that the electron ionization time of the molecule is very sensitive to the angular-dependent ionization rate.

Except for the emission angle of the most probable electron trajectory, the angular width of the PAD is another significant quantity to characterize the overall structure of the PMD in the attoclock configuration [18]. We show in Fig. 4(a) the measured full width at half maximum (FWHM) of the PADs as a function of the alignment angle for N_2 and CO_2. For N_2, the alignment dependence of the FWHM shows two peaks at $\theta = 90^\circ$ and 270°, while for CO_2 there are four peaks at $\theta = 0^\circ$, 90°, 180°, and 270°. The simulation using the deconvoluted angular-dependent ionization rate is shown in Fig. 4(b), which is consistent with the measurement.

The alignment dependence of the angular width can be understood with two-center electron interference, as predicted by Serov *et al.* [18]. The PAD can be regarded as a product of an angular distribution from a single center emission and a two-center interference factor. The two-center interference factor can be written as [18,36] $P_{tc} \propto \cos^2(\frac{\mathbf{kR}}{2} + \frac{\Delta\Phi}{2})$, where $\mathbf{R}$ is the internuclear distance and the phase difference is $\Delta\Phi = 0$ for a bonding orbital and $\Delta\Phi = \pi$ for an antibonding orbital [37]. For the N_2 molecule, the HOMO can be approximated by a linear combination of two atomic p_z orbitals (z indicates molecular axis direction) [38]; thus the PAD is expressed as $P \propto P_{sc}\cos^2[\frac{kR}{2}\cos(\phi - \theta)]$, where P_{sc} indicates the single center emission. For the minor axis molecular alignment ($\theta = 90^\circ$ or 270°), a destructive two-center interference at the emission angle of $\sim 90^\circ$ leads to a considerable increase of the width of the PMD [18]. For the CO_2 molecule, its HOMO is very similar to that of O_2, which can be approximated by a linear combination of two atomic p_x orbitals [38]. As a result, the PAD can be expressed as $P \propto \sin^2(\phi - \theta)\sin^2[\frac{kR}{2}\cos(\phi - \theta)]$, where $\sin^2(\phi - \theta)$ comes from the single center emission, leading to an increase of the angular width at $\theta = 0^\circ$, 90°, 180°, and 270°. Thus the angular width of the PADs is mainly determined by two-center interference, confirming the predictions by Serov *et al.* [18], and it is also strongly affected by the single center emission.

IV. CONCLUSION

In summary, we have measured the alignment-dependent PADs for N_2 and CO_2 in the attoclock configuration. We find that in molecules the electron ionization time corresponding to the peak of the PMD shifts several tens of attoseconds relative to the laser field peak depending on the molecular orientation and molecular orbital structure. This finding has a strong impact on the interpretation of attoclock experiments for molecules. We further demonstrate that the photoelectron ionization time in molecules is sensitive to the angular-dependent ionization rate, providing an alternative way of probing attosecond electron dynamics in complex polyatomic molecules. In a complex polyatomic molecule, the valence electron is weakly bound. Thus the HOMO or inner orbitals of the polyatomic molecule can be deformed by the instantaneous electric field of a strong laser pulse, which will leave a fingerprint on the angular-dependent ionization rate [39]. Due to the sensitivity of the photoelectron ionization time to the angular-dependent ionization rate, the ultrafast laser-induced orbital deformation might be directly observed with the molecular attoclock technique.

ACKNOWLEDGMENTS

This work is supported by the National Natural Science Foundation of China (Grants No. 11722432, No. 11674116, and No. 61475055) and National Key Research and Development Program of China (Grant No. 2019YFA0308300).

J.Y. and W.X. contributed equally to this work.

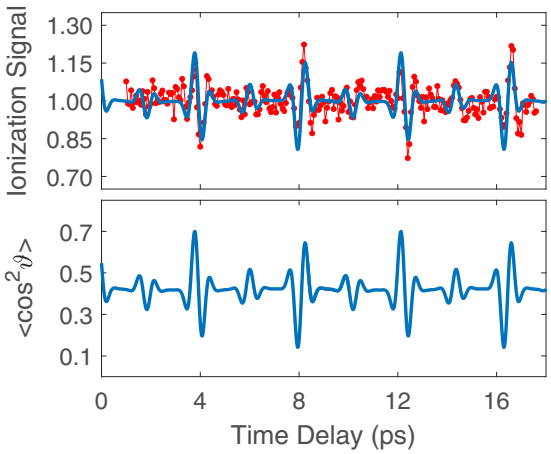

FIG. 5. The measured ionization signals (the red dots in the upper panel) and the corresponding degree of alignment $\langle\cos^2\vartheta\rangle$ (lower panel) of N_2 with respect to the time delay between two linearly polarized laser pulses. For comparison, the ionization signals calculated by the deconvoluted ionization rate are shown by the blue line in the left-hand panel.

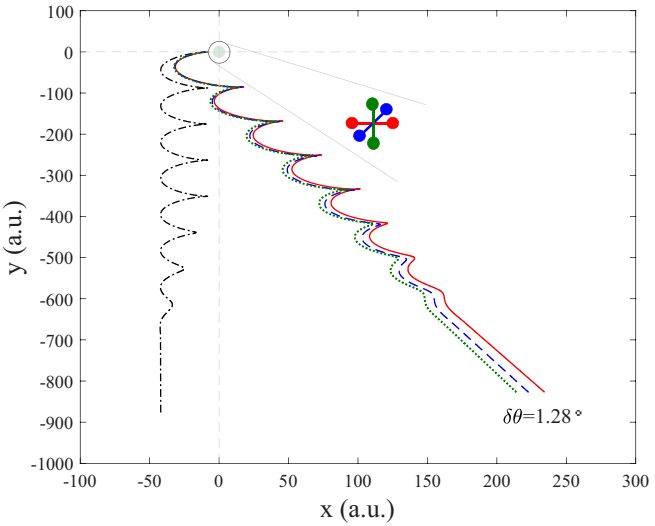

FIG. 6. The simulated classical trajectories correspond to different alignment angles of 0° (solid red line), 45° (dashed blue line), and 90° (dotted green line) by solving the classical Newtonian equation. The dash-dotted black line is the trajectory with neglecting the Coulomb interaction. The emission angle difference for different alignments is smaller than 1.3°.

APPENDIX A: DEGREES OF ALIGNMENT FOR THE MOLECULES

When a molecule (N_2 or CO_2) is placed in a femtosecond laser pulse, a time-dependent rotational wave packet Ψ will be excited from the initial state. To obtain the degrees of alignment, we solve the time-dependent Schrödinger equation (TDSE) with the rigid-rotor approximation [27,40],

$$i\frac{\partial\Psi(\vartheta,\varphi;\tau)}{\partial t}=\left[BJ^2-\frac{E(\tau)^2}{2}(\Delta\alpha\cos^2\vartheta+\alpha_\perp)\right]\Psi(\vartheta,\varphi;\tau), \tag{A1}$$

where ϑ is the alignment angle between the molecular axis and the polarization direction of the alignment beam, φ is the azimuthal angle in the frame of the alignment beam, B is the rotational constant, J is the angular momentum operator, $E(\tau)$ is the time-dependent laser field of the alignment pulse, and $\Delta\alpha=\alpha_\parallel-\alpha_\perp$ is the polarizability difference between the parallel components $\alpha_\parallel$ and perpendicular components $\alpha_\perp$ relative to the molecular axis. For N_2, $B=1.989\ \mathrm{cm}^{-1}$, $\alpha_\parallel=2.38\ \text{Å}^3$, and $\alpha_\perp=1.45\ \text{Å}^3$ [41]. For CO_2, $B=0.39\ \mathrm{cm}^{-1}$, $\alpha_\parallel=4.05\ \text{Å}^3$, and $\alpha_\perp=1.95\ \text{Å}^3$ [41]. The three-dimensional degree of alignment is calculated by $\langle\cos^2\vartheta\rangle=\langle\Psi|\cos^2\vartheta|\Psi\rangle$. If there is no alignment pulse, $\langle\cos^2\vartheta\rangle=1/3$.

We take N_2 molecules as an example. In the experiment, the intensity of the alignment pulse is estimated to be about $3.1\times10^{13}\ \mathrm{W/cm}^2$. The degree of alignment calculated by the TDSE is shown in the lower panel of Fig. 5 as a function of the time delay. The upper panel of Fig. 5 shows the measured photoelectron yield as a function of the time delay (the red dots). One can see that the time dependence of the photoelectron yield shows a strong similarity with the theoretical curve in the lower panel. In our molecular attoclock experiment, the time delay between the probe pulse and the alignment pulse is set to be 8.33 ps, at which the degree of alignment is almost $\langle\cos^2\vartheta\rangle\approx0.65$ for N_2. We also calculate the time-dependent ionization signals $\langle\Psi|w|\Psi\rangle$ using the deconvoluted ionization rate of N_2 molecules (see Appendix C for details). As shown by the blue curve in the upper panel of Fig. 5, the calculation agrees well with the measurement.

APPENDIX B: THE EFFECT OF THE COULOMB POTENTIAL ON THE ELECTRON EMISSION ANGLE

In extracting the photoelectron ionization time of a molecule from the emission angle, we assumed that the Coulomb potential leads to constant angular shift for different molecular orientations. To justify this assumption, we have calculated classical trajectories corresponding to different alignment angles using a simple model. In this model, the position of the tunnel exit is determined by $V(x)+xE_0=-I_p$. The initial momentum at the tunnel exit is assumed to be zero. After tunneling, the motion of the trajectory is described by the classical Newtonian equation,

$$\frac{\partial^2\mathbf{r}}{\partial t^2}=-\nabla[V(\mathbf{r})+\mathbf{r}\cdot\mathbf{E}(t)]. \tag{B1}$$

The electric field $\mathbf{E}(t)$ has a trapezoidal envelope which has eight optical cycles in total with four cycles ramping off. The model potential for the N_2 molecule is given by $V(\mathbf{r})=-\frac{Z}{|\mathbf{r}-\mathbf{R_0}/2|}-\frac{Z}{|\mathbf{r}+\mathbf{R_0}/2|}$, where $\mathbf{R_0}$ is the internuclear separation vector ($R_0=2.07$ a.u. for N_2) and $Z=1/2$. As shown in Fig. 6, the classical trajectories of the electron after tunneling from N_2 are shown for different alignment angles of 0°, 45°, and 90°. For comparison, we also show the classical trajectory without including the molecular potential (dash-dotted black line). One can see that the Coulomb potential leads to a large angular shift for the emission angle of the photoelectron. However, for different alignment angles, the difference of the emission angle induced by the Coulomb potential is very small. This implies that the photoelectron ionization time of

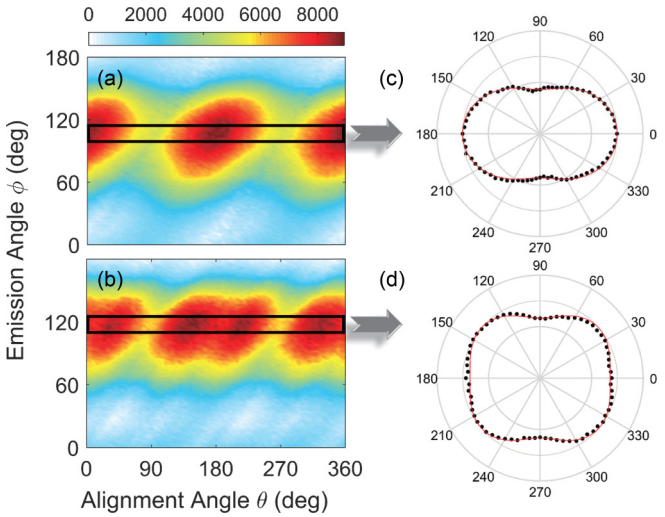

FIG. 7. The photoelectron angular distributions of (a) N_2 and (b) CO_2 with respect to the alignment angle. The photoelectrons released at around the major axis of the laser ellipse (framed black) are used to retrieve the angular-dependent ionization rate. The measured photoelectron yield $M(\theta)$ released near the major axis of the elliptically polarized field as a function of the angle θ between the major axis of the probe pulse and alignment pulse for (c) N_2 and (d) CO_2. The solid red lines in (c) and (d) are the best fits using the corresponding functional forms.

molecules can be extracted without counting on the theoretical modeling of the Coulomb effect.

APPENDIX C: DECONVOLUTION PROCESS TO OBTAIN THE ANGULAR-DEPENDENT IONIZATION RATE

When a molecule (N_2 or CO_2) is ionized, the measured angular-dependent ionization signal $M(\theta)$ can be written as the convolution of the angular-dependent ionization rate $S(\beta)$ with the alignment distribution $A(\vartheta, \varphi)$ [21],

$$M(\theta) = \int_{\varphi=0}^{2\pi} \int_{\vartheta=0}^{\pi} S[\beta(\vartheta, \varphi; \theta)] A(\vartheta, \varphi) \sin(\vartheta)\, d\vartheta\, d\varphi, \tag{C1}$$

where the angle β between the polarization axis of the instantaneous ionizing field and the molecular axis is given by $\cos\beta = \cos\theta\cos\vartheta - \sin\theta\sin\vartheta\sin\varphi$. Here φ is the polar angle in the frame of the alignment beam, and θ is the angle between the instantaneous ionizing beam and the alignment beam. The alignment distribution $A(\vartheta, \varphi)$ is calculated by $A(\vartheta, \varphi) = |\Psi|^2$, where Ψ is obtained by solving Eq. (A1).

In the experiment, an elliptically polarized intense laser pulse was used to ionize N_2 and CO_2. We follow the procedure in Ref. [21] to retrieve the angular-dependent ionization rate $S(\beta)$ using the photoelectrons released around the major axis of the laser ellipse. As shown in Figs. 7(a) and 7(b), the photoelectron angular distributions are shown with respect to the alignment angle for N_2 and CO_2 [the same as in Figs. 2(a) and 2(b)]. The maximum ionization rate corresponds to the electrons released near the field maximum (near the major axis of the elliptically polarized laser field) at each alignment angle (framed black). The yields of those electrons as a function of the alignment angle $M(\theta)$ are shown in Figs. 7(c) and 7(d), which are very similar to the results in Ref. [21].

To retrieve the angular-dependent ionization rate $S(\beta)$ from the measured yields $M(\theta)$ [Figs. 7(c) and 7(d)], we write $S(\beta) = \sum_{m=0}^{3} C_m \cos(2m\beta)$ and $S(\beta) = \cos^n(\beta - \beta_m) + \cos^n(\beta + \beta_m)$ for N_2 and CO_2 [21], respectively. Here C_m, β_m, and n are adjustable coefficients. Then those coefficients are determined when the calculated $M(\theta)$ is best fit with the measured $M(\theta)$. As shown in Figs. 7(c) and 7(d), the best fits using the corresponding functional forms are shown by the solid red lines. As a result, we obtain the angular-dependent ionization $S(\beta)$ for N_2 and CO_2, as shown in Figs. 3(c) and 3(d) of the main text, which deviate noticeably from the MO-ADK results [17].

Using the retrieved angular-dependent ionization rate $S(\beta)$, we calculate the most probable electron emission angle in an elliptically polarized laser field. Generally, the instantaneous ionization rate of a molecule in an elliptically polarized laser field $S(\beta, E(t))$ depends on the magnitude of the electric field and the alignment angle. For simplicity, this instantaneous ionization rate can be approximately written as a product of the angular-dependent ionization rate at constant electric field strength and a factor related to the instantaneous electric field, i.e.,

$$S(\beta, E(t)) = S(\beta) W(E(t)), \tag{C2}$$

where $W(E(t))$ can be estimated by the ADK rate of an atom [29], i.e., $W(E(t)) \propto e^{\frac{-2\kappa^3}{3}\left(\frac{1}{E(t)} - \frac{1}{E_0}\right)}$ with $\kappa = \sqrt{2I_p}$, where I_p is the ionization potential. From Eq. (C2), we can obtain the ionization time t_0 for the most probable electron trajectory. The emission angle of the most probable electron trajectory is determined by the final momentum $\mathbf{k} \approx -\mathbf{A}(t_0)$, where $\mathbf{A}(t)$ is the vector potential of the laser field.

[1] F. Krausz and M. Ivanov, Rev. Mod. Phys. **81**, 163 (2009).

[2] P. Eckle, A. N. Pfeiffer, C. Cirelli, A. Staudte, R. Dörner, H. G. Muller, M. Büttiker, and U. Keller, Science **322**, 1525 (2008).

[3] H. Ni, U. Saalmann, and J.-M. Rost, Phys. Rev. Lett. **117**, 023002 (2016).

[4] A. S. Landsman, M. Weger, J. Maurer, R. Boge, A. Ludwig, S. Heuser, C. Cirelli, L. Gallmann, and U. Keller, Optica **1**, 343 (2014).

[5] L. Torlina, F. Morales, J. Kaushal, I. Ivanov, A. Kheifets, A. Zielinski, A. Scrinzi, H. G. Muller, S. Sukiasyan, M. Ivanov, and O. Smirnova, Nat. Phys. **11**, 503 (2015).

[6] N. Camus, E. Yakaboylu, L. Fechner, M. Klaiber, M. Laux, Y. Mi, K. Z. Hatsagortsyan, T. Pfeifer, C. H. Keitel, and R. Moshammer, Phys. Rev. Lett. **119**, 023201 (2017).

[7] U. Sainadh, H. Xu, X. Wang, A. Atia-Tul-Noor, W. Wallace, N. Douguet, A. Bray, I. Ivanov, K. Bartschat, A. Kheifets, R. Sang, and I. Litvinyuk, Nature (London) **568**, 75 (2019).

[8] C. Hofmann, A. S. Landsman, and U. Keller, J. Mod. Opt. **66**, 1052 (2019).
[9] J. M. Rost and U. Saalmann, Nat. Photonics **13**, 439 (2019).
[10] M. Meckel, A. Staudte, S. Patchkovkii, D. M. Villeneuve, P. B. Corkum, R. Dörner, and M. Spanner, Nat. Phys. **10**, 594 (2014).
[11] M.-M. Liu, M. Li, C. Wu, Q. Gong, A. Staudte, and Y. Liu, Phys. Rev. Lett. **116**, 163004 (2016).
[12] M. He, Y. Li, Y. Zhou, M. Li, W. Cao, and P. Lu, Phys. Rev. Lett. **120**, 133204 (2018).
[13] J. Wu, M. Magrakvelidze, L. P. H. Schmidt, M. Kunitski, T. Pfeifer, M. Schöffler, M. Pitzer, M. Richter, S. Voss, H. Sann, H. Kim, J. Lower, T. Jahnke, A. Czasch, U. Thumm, and R. Dörner, Nat. Commun. **4**, 2177 (2013).
[14] A. Khan, D. Trabert, S. Eckart, M. Kunitski, T. Jahnke, and R. Dörner, Phys. Rev. A **101**, 023409 (2020).
[15] W. Quan, V. V. Serov, M. Z. Wei, M. Zhao, Y. Zhou, Y. L. Wang, X. Y. Lai, A. S. Kheifets, and X. J. Liu, Phys. Rev. Lett. **123**, 223204 (2019).
[16] A. H. Winney, S. K. Lee, Y. F. Lin, Q. Liao, P. Adhikari, G. Basnayake, H. B. Schlegel, and W. Li, Phys. Rev. Lett. **119**, 123201 (2017).
[17] X. M. Tong, Z. X. Zhao, and C. D. Lin, Phys. Rev. A **66**, 033402 (2002).
[18] V. V. Serov, A. W. Bray, and A. S. Kheifets, Phys. Rev. A **99**, 063428 (2019).
[19] R. Dörner, V. Mergel, O. Jagutzki, L. Spielberger, J. Ullrich, R. Moshammer, and H. Schmidt-Böcking, Phys. Rep. **330**, 95 (2000).
[20] J. Ullrich, R. Moshammer, A. Dorn, R. Dörner, L. Ph. H. Schmidt, and H. Schmidt-Böcking, Rep. Prog. Phys. **66**, 1463 (2003).
[21] D. Pavičić, K. F. Lee, D. M. Rayner, P. B. Corkum, and D. M. Villeneuve, Phys. Rev. Lett. **98**, 243001 (2007).
[22] J. Yao, G. Li, X. Jia, X. Hao, B. Zeng, C. Jing, W. Chu, J. Ni, H. Zhang, H. Xie, C. Zhang, Z. Zhao, J. Chen, X. Liu, Y. Cheng, and Z. Xu, Phys. Rev. Lett. **111**, 133001 (2013).
[23] K. Liu, S. Luo, M. Li, Y. Li, Y. Feng, B. Du, Y. Zhou, P. Lu, and I. Barth, Phys. Rev. Lett. **122**, 053202 (2019).
[24] S. Luo, M. Li, W. Xie, K. Liu, Y. Feng, B. Du, Y. Zhou, and P. Lu, Phys. Rev. A **99**, 053422 (2019); K. Liu, M. Li, W. Xie, K. Guo, S. Luo, J. Yan, Y. Zhou, and P. Lu, Opt. Express **28**, 12439 (2020).
[25] M. Li, M.-M. Liu, J.-W. Geng, M. Han, X. Sun, Y. Shao, Y. Deng, C. Wu, L.-Y. Peng, Q. Gong, and Y. Liu, Phys. Rev. A **95**, 053425 (2017).
[26] T. Seideman, J. Chem. Phys. **103**, 7887 (1995).
[27] J. Ortigoso, M. Rodriguez, M. Gupta, and B. Friedrich, J. Chem. Phys. **110**, 3870 (1999).
[28] I. A. Ivanov, C. Hofmann, L. Ortmann, A. S. Landsman, C. H. Nam, and K. T. Kim, Commun. Phys. **1**, 81 (2018).
[29] M. V. Ammosov, N. B. Delone, and V. P. Krainov, Sov. Phys. JETP **64**, 1191 (1986).
[30] S. Petretti, Y. V. Vanne, A. Saenz, A. Castro, and P. Decleva, Phys. Rev. Lett. **104**, 223001 (2010).
[31] S.-K. Son and Shih-I Chu, Phys. Rev. A **80**, 011403(R) (2009).
[32] V. P. Majety and A. Scrinzi, Phys. Rev. Lett. **115**, 103002 (2015).
[33] R. Murray, M. Spanner, S. Patchkovskii, and M. Yu. Ivanov, Phys. Rev. Lett. **106**, 173001 (2011).
[34] M. D. Śpiewanowski and L. B. Madsen, Phys. Rev. A **91**, 043406 (2015).
[35] I. Thomann, R. Lock, V. Sharma, E. Gagnon, S. T. Pratt, H. C. Kapteyn, M. M. Murnane, and W. Li, J. Phys. Chem. A **112**, 9382 (2008).
[36] M. Kunitski, N. Eicke, P. Huber, J. Köhler, S. Zeller, J. Voigtsberger, N. Schlott, K. Henrichs, H. Sann, F. Trinter, L. Ph. H. Schmidt, A. Kalinin, M. S. Schöffler, T. Jahnke, M. Lein, and R. Dörner, Nat. Commun. **10**, 1 (2019).
[37] J. Muth-Böhm, A. Becker, and F. H. M. Faisal, Phys. Rev. Lett. **85**, 2280 (2000).
[38] V. I. Usachenko and S.-I. Chu, Phys. Rev. A **71**, 063410 (2005).
[39] H. Akagi, T. Otobe, and R. Itakura, Sci. Adv. **5**, eaaw1885 (2019).
[40] T. Seideman, Phys. Rev. Lett. **83**, 4971 (1999).
[41] C. Jin, A. T. Le, S. F. Zhao, R. R. Lucchese, and C. D. Lin, Phys. Rev. A **81**, 033421 (2010).